Supporting Information

Salt-assisted in-situ formation of N-doped porous carbons for boosting k^+ storage capacity and cycling stability

Wen-zhe Zhang, Huan-lei Wang *, Ran-xia Liao, Wen-rui Wei, Xue-chun Li, Shuai Liu, Ming-hua Huang, Zhi-cheng Shi, Jing Shi *

(School of Materials Science and Engineering, Ocean University of China, Qingdao 266100, China)

Corresponding author: E-mail：huanleiwang@gmail.com (H. Wang)
E-mail：shijing@ouc.edu.cn (J. Shi)

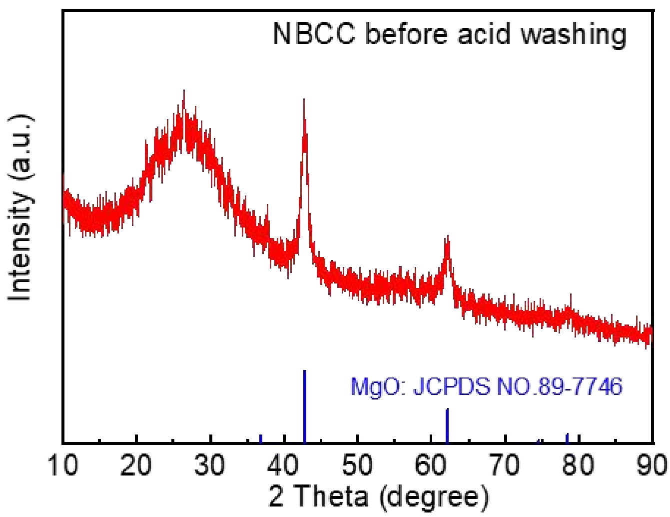

Fig. S1 XRD patterns of the NBCC sample before washing with HCl.

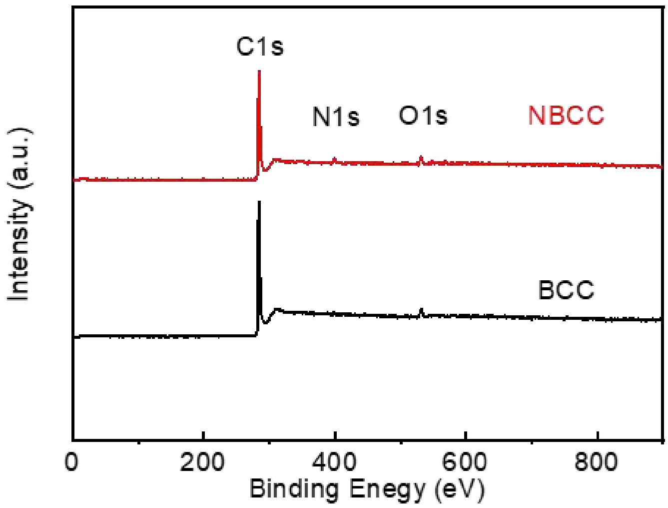

Fig. S2 (a) XPS survey spectra of BCC and NBCC.

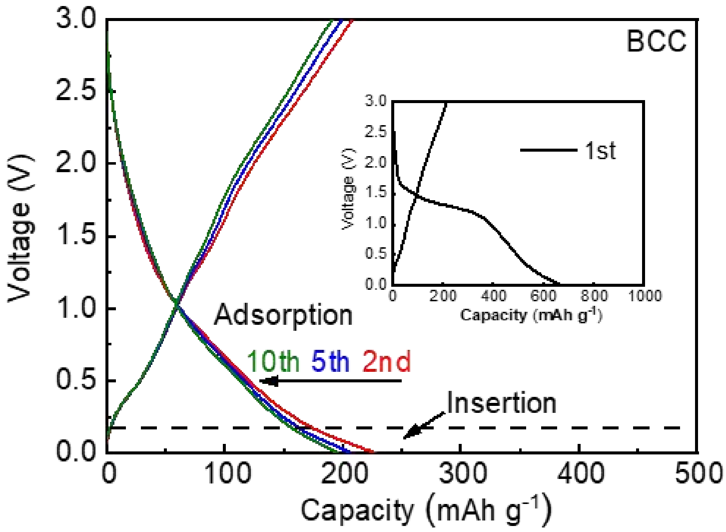

Fig. S3 Galvanostatic discharge-charge profiles of BCC at 0.05 A g^{-1}.

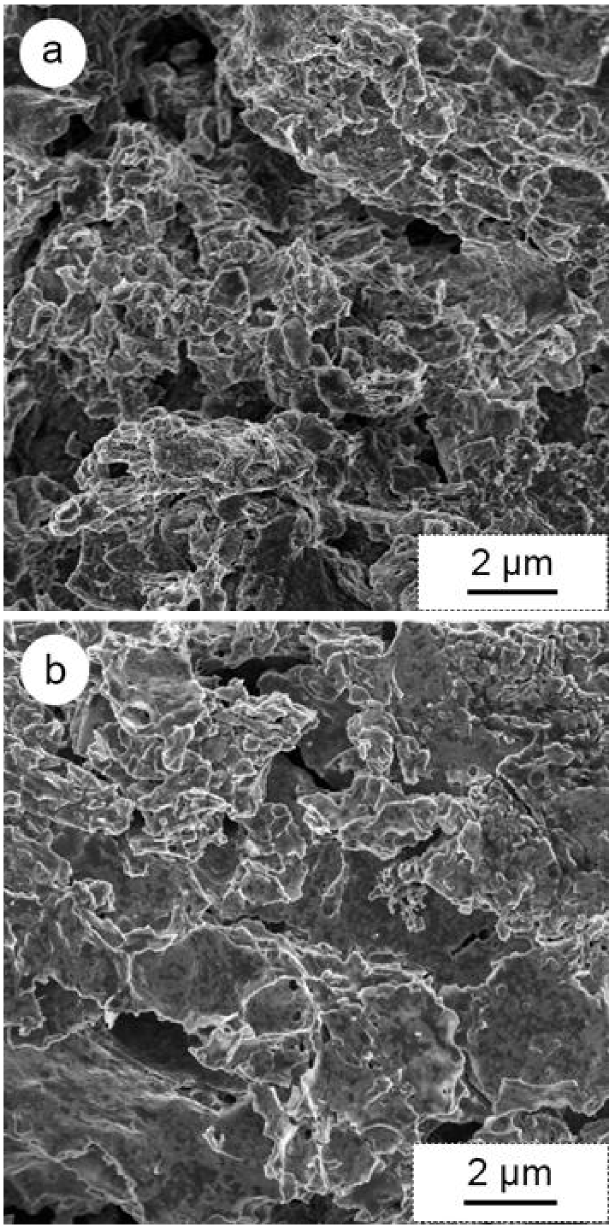

Fig. S4 The SEM images of NBCC (a) after 100 cycles, and (b) after 1000 cycles.

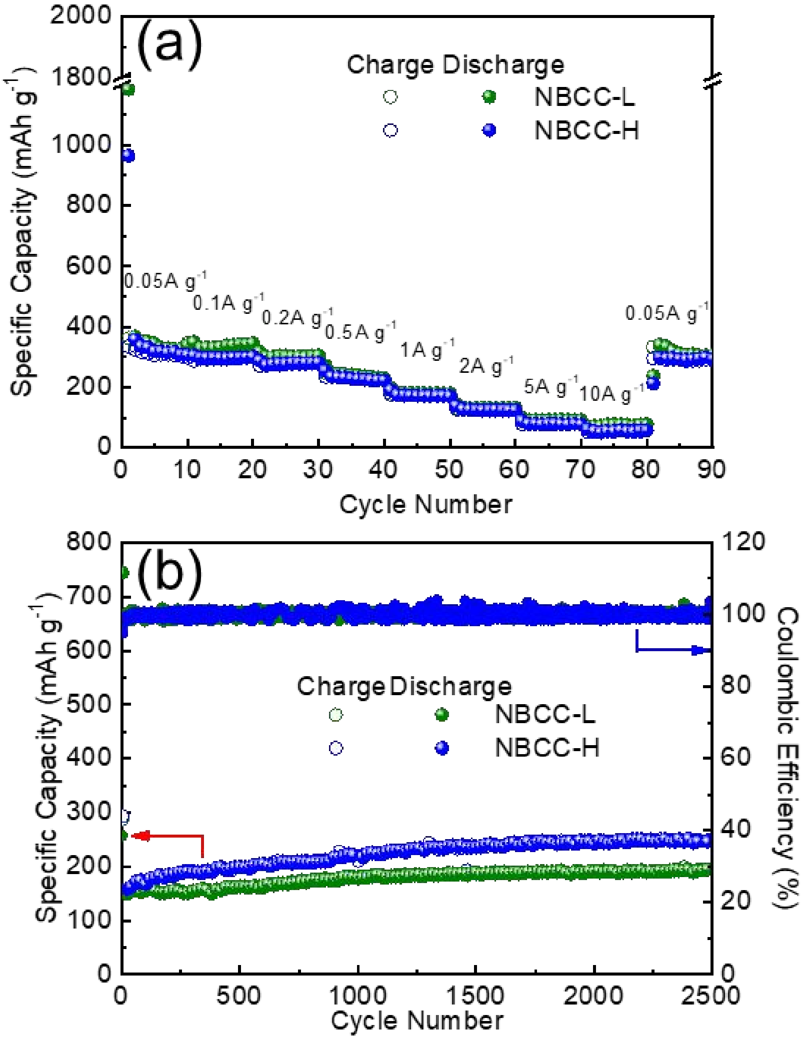

Fig. S5 (a) Rate capability, and (b) Long cycling performance at 2.0 A g^{-1} of NBCC-L and NBCC-H electrodes.

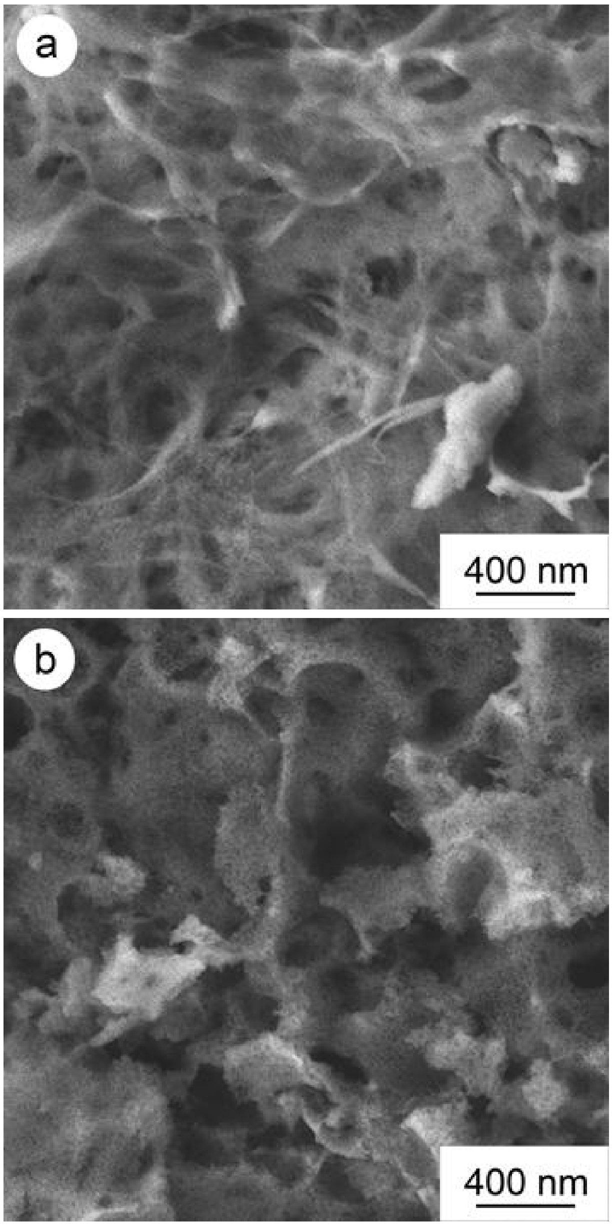

Fig. S6 SEM images of (a) NBCC-L and (b) NBCC-H.

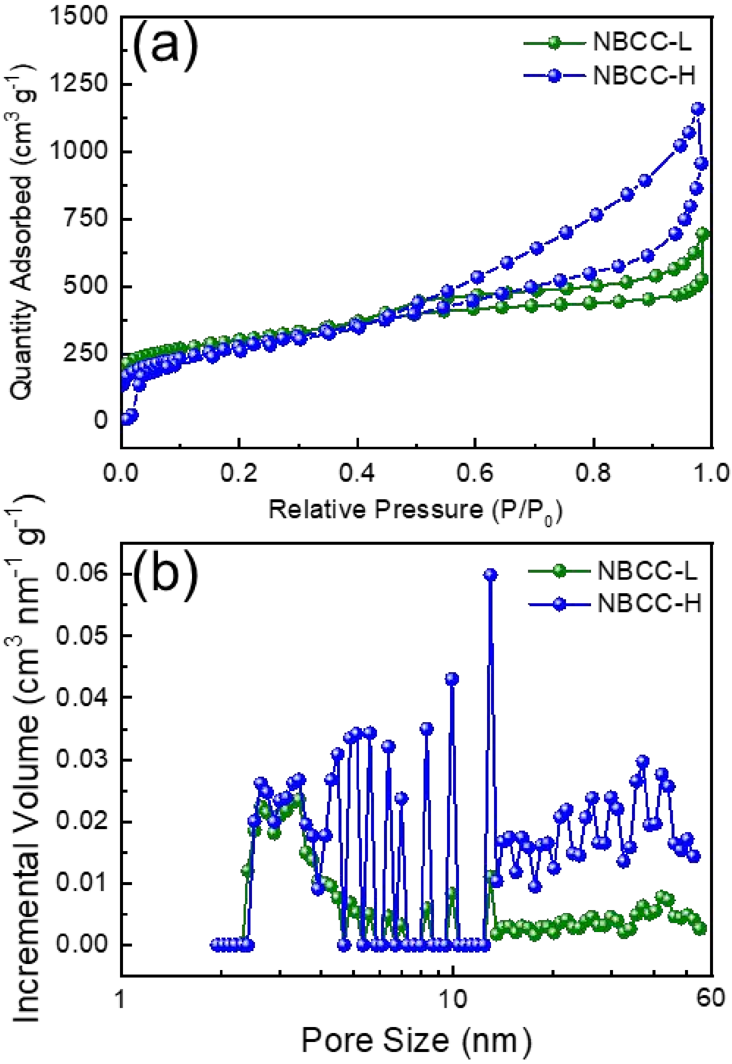

Fig. S7 (a) Nitrogen adsorption-desorption isothermal curves, and (b) DFT pore size distribution of NBCC-L and NBCC-H.

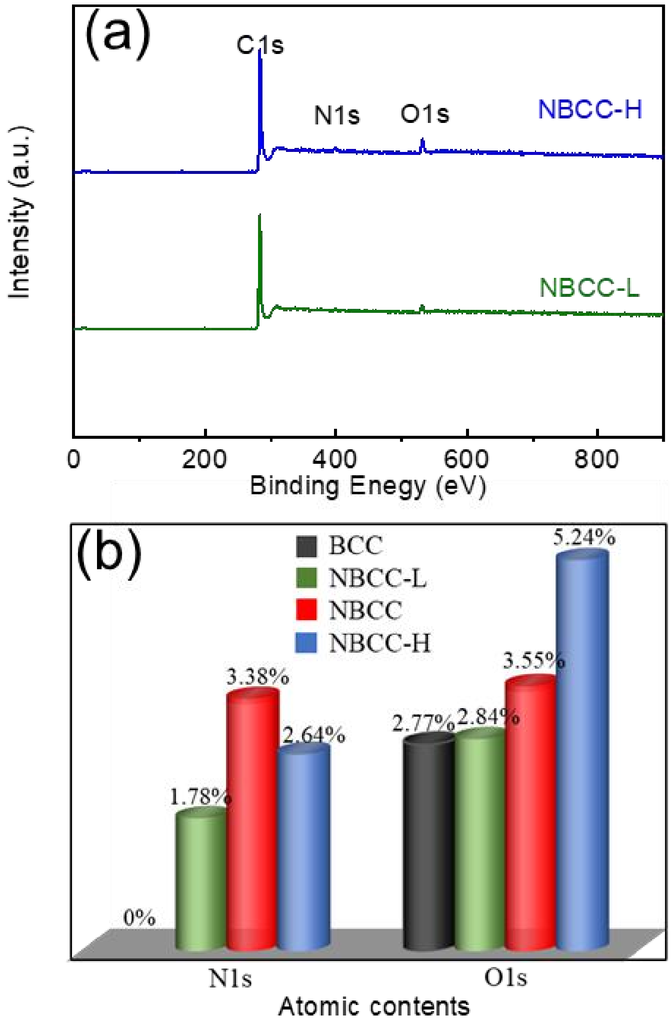

Fig. S8 (a) XPS survey spectra of NBCC-L and NBCC-H. (b) atomic contents of N/O elements of BCC, NBCC, NBCC-L and NBCC-H.

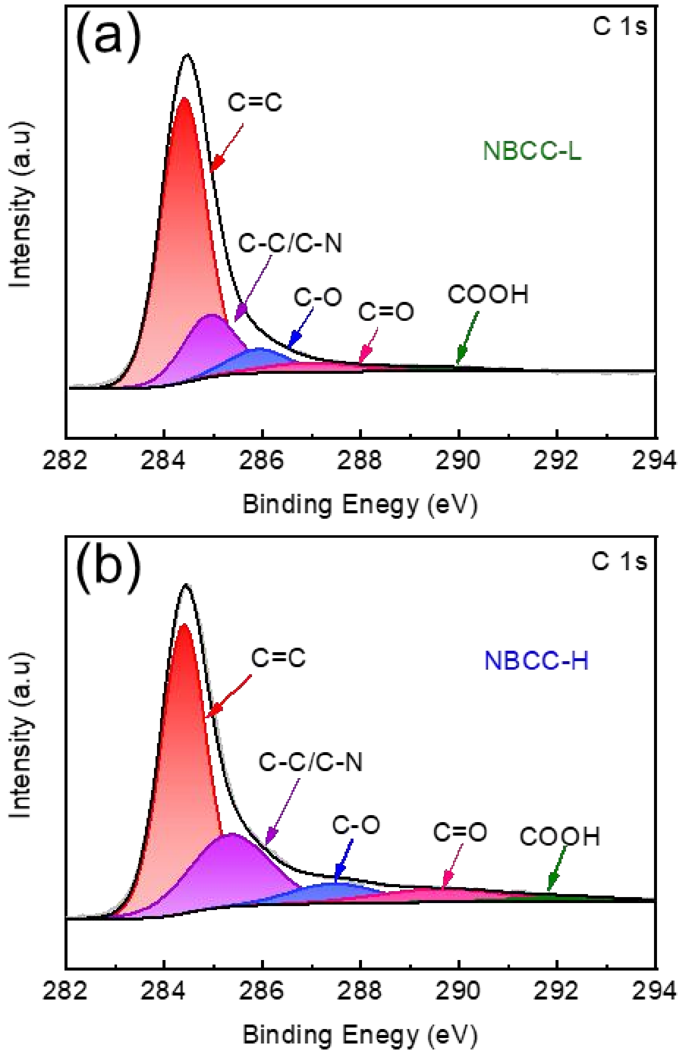

Fig. S9 C 1s spectra of (a) NBCC-L and (b) NBCC-H.

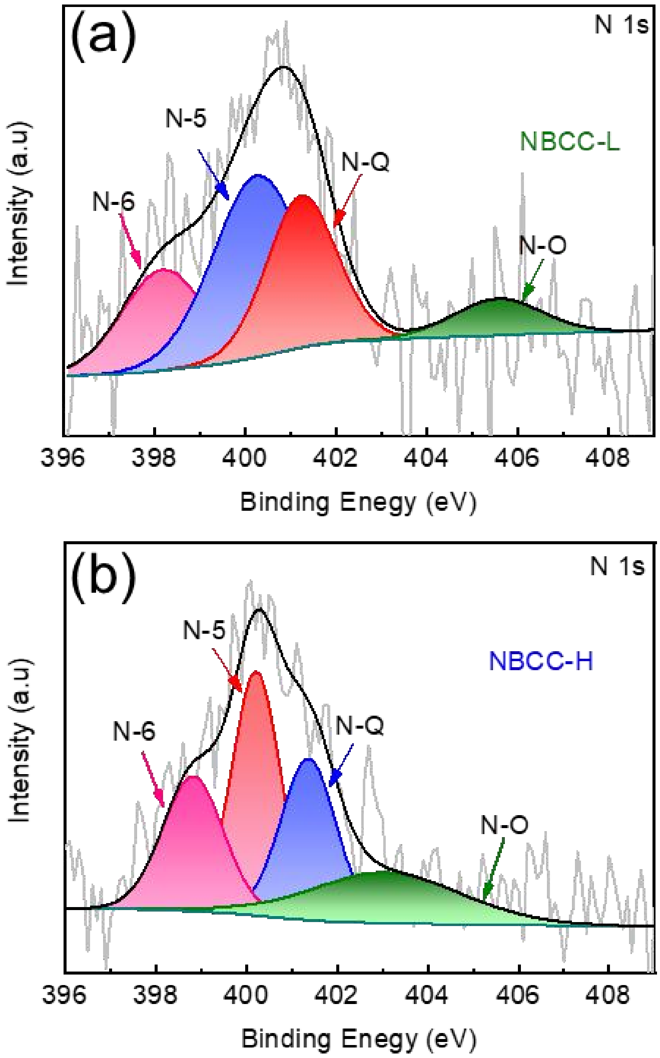

Fig. S10 N 1s spectra of (a) NBCC-L and (b) NBCC-H.

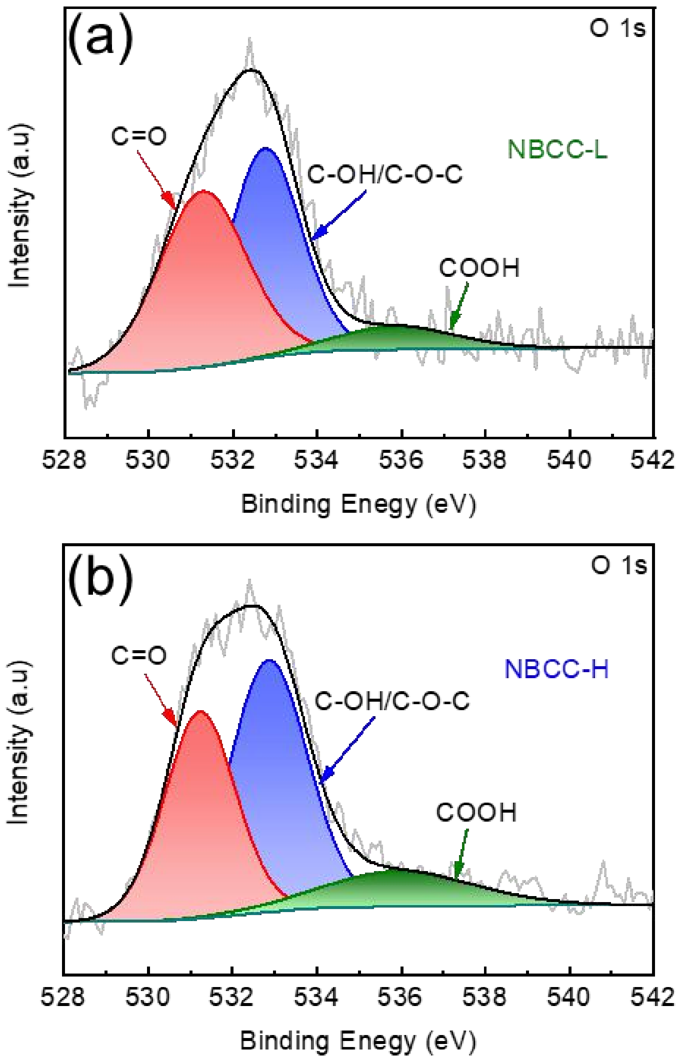

Fig. S11 O 1s spectra of (a) NBCC-L and (b) NBCC-H.

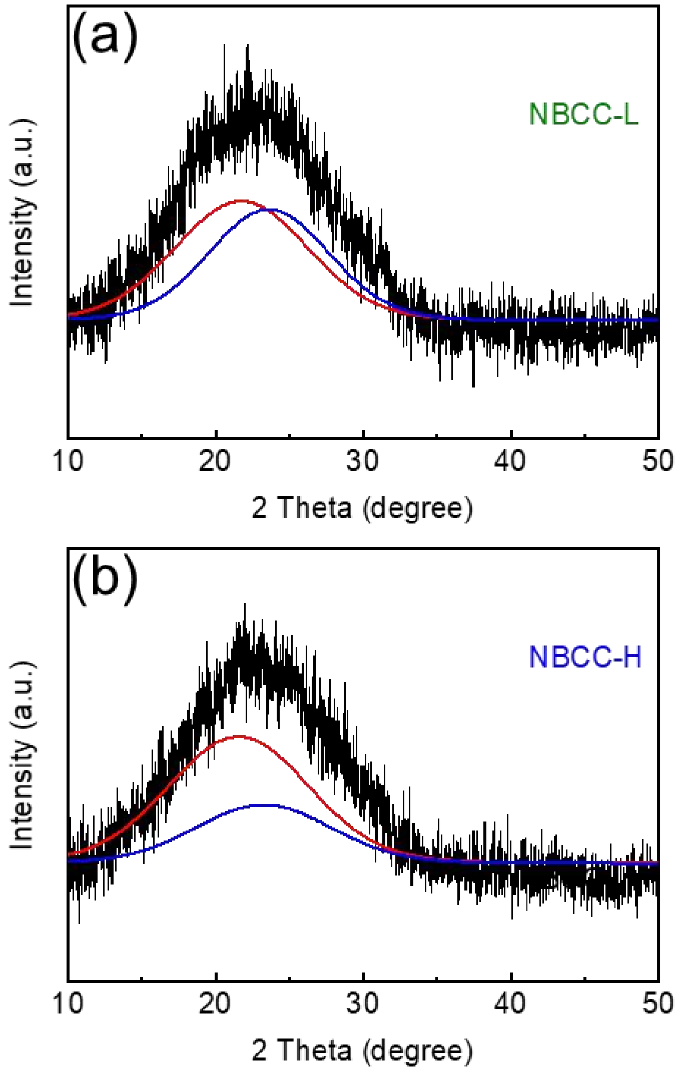

Fig. S12 XRD pattern of (a) NBCC-L and (b) NBCC-H.

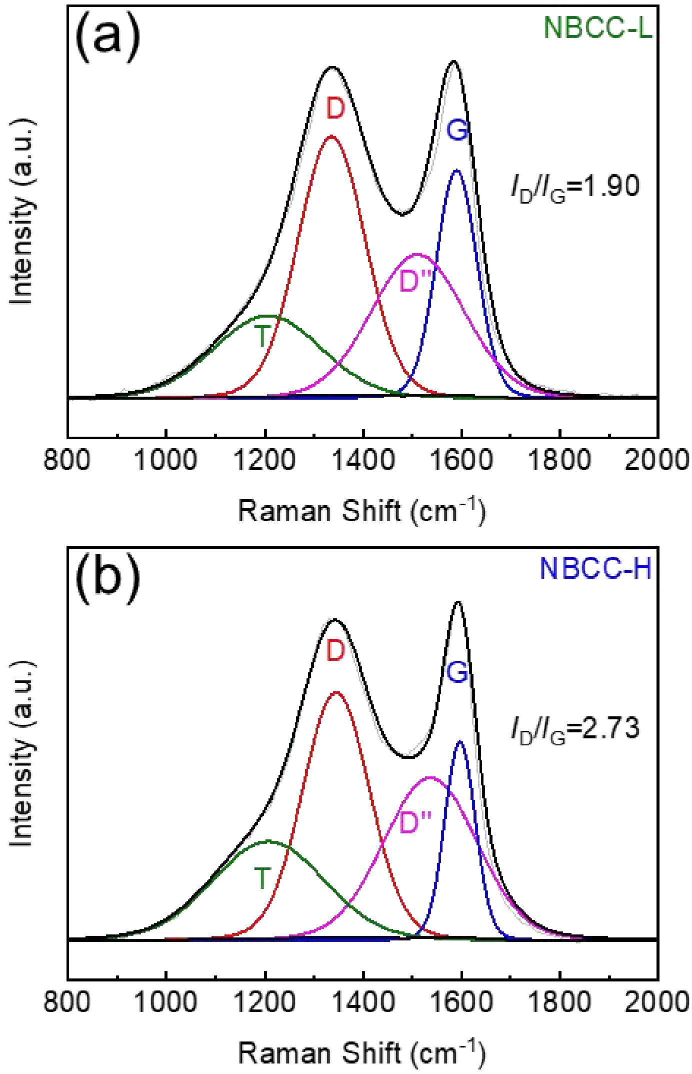

Fig. S13 Raman spectra of (a) NBCC-L and (b) NBCC-H.

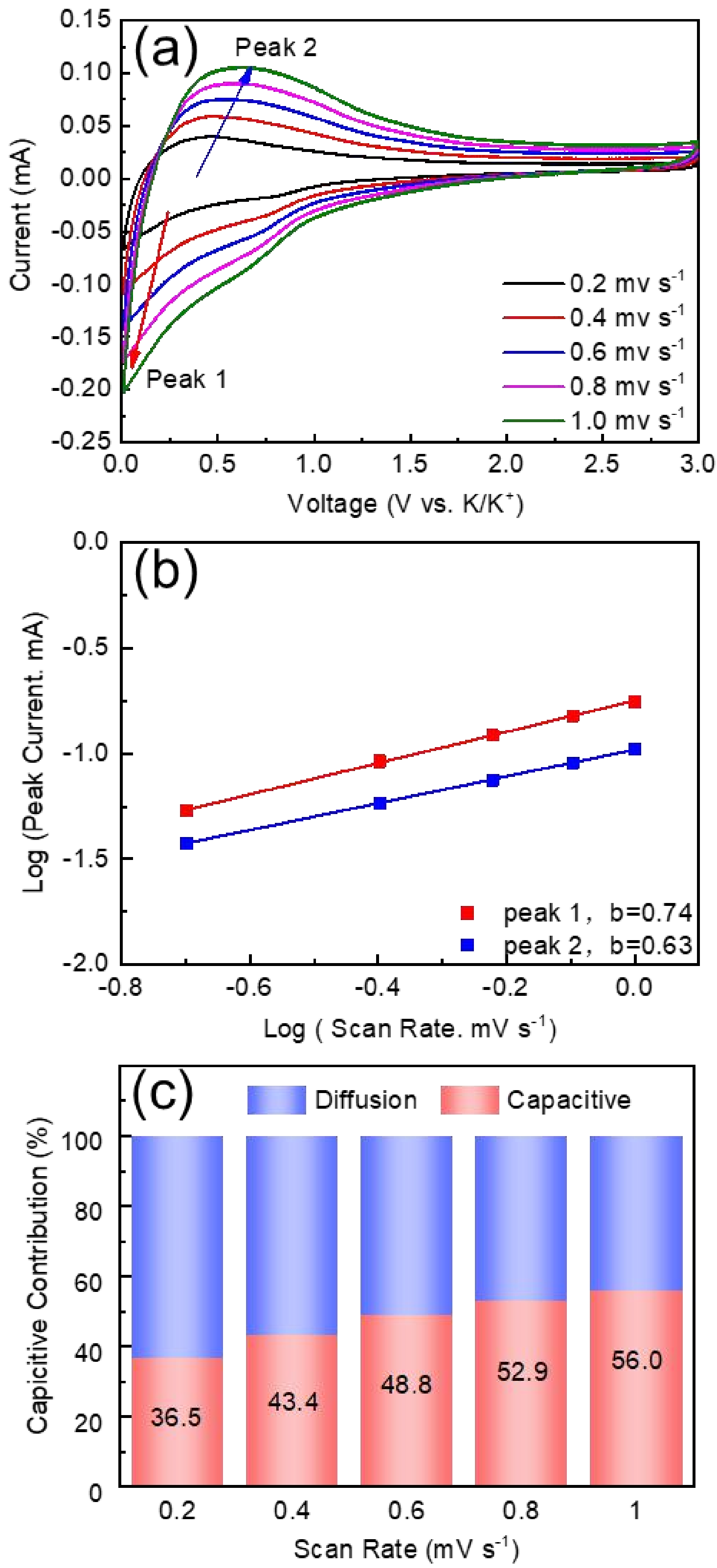

Fig. S14 (a) CV curves at different scan rates, (b) Fitted line between log(i) and log(v), (c) Normalized capacitive contribution ratio of BCC at different scan rates.

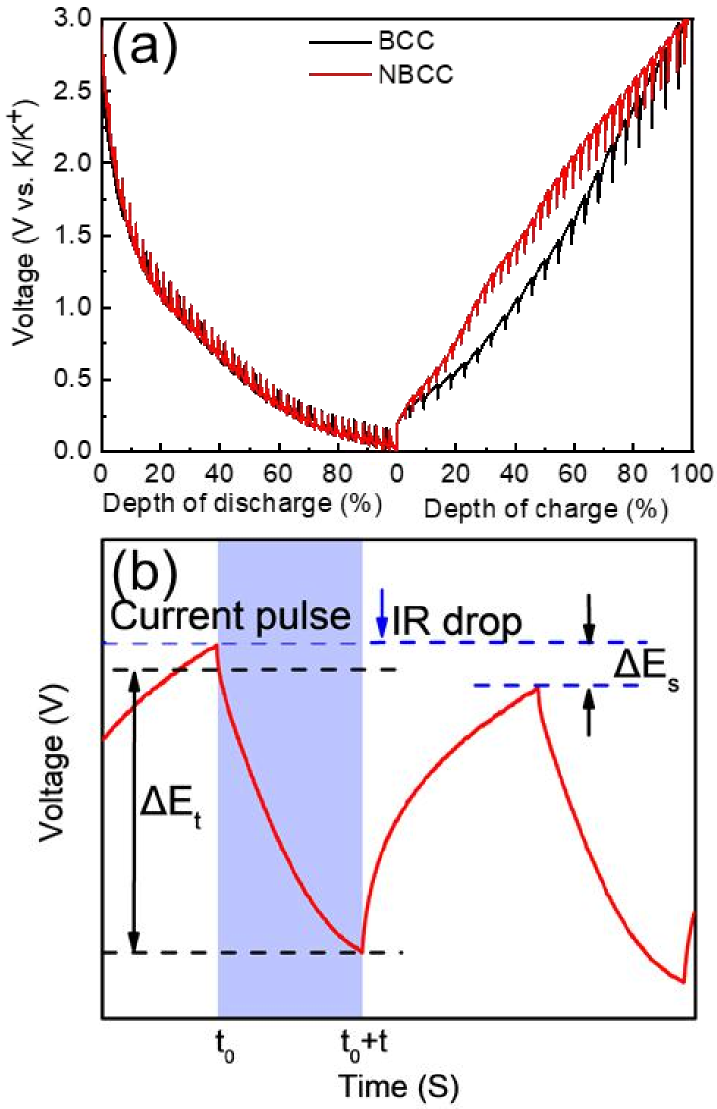

Fig. S15 (a) GITT curves and (b) the schematic illustration for the GITT calculation method of BCC and NBCC.

The GITT profiles to investigate the K-ion diffusion coefficient (D_k) during cycling via discharging/charging at 0.03 A g^{-1} for 30 min followed by an open-circuit relaxation for 180 min. The D_k value can be calculated according to the Fick's second law and the equation (S1):

$$D_{Na} = \frac{4}{\pi\tau}\left(\frac{m_B V_M}{M_b S}\right)^2\left(\frac{\Delta E_s}{\Delta E_t}\right)^2 \quad \text{(S1)}$$

where τ is the pulse time (s), m_B is the mass of the active materials, M_b is the molar mass of the active material, V_M represents the molar volume of the active material, S is the geometric area of the electrode, and ΔE_s and ΔE_t are defined as shown in Figure S12b.

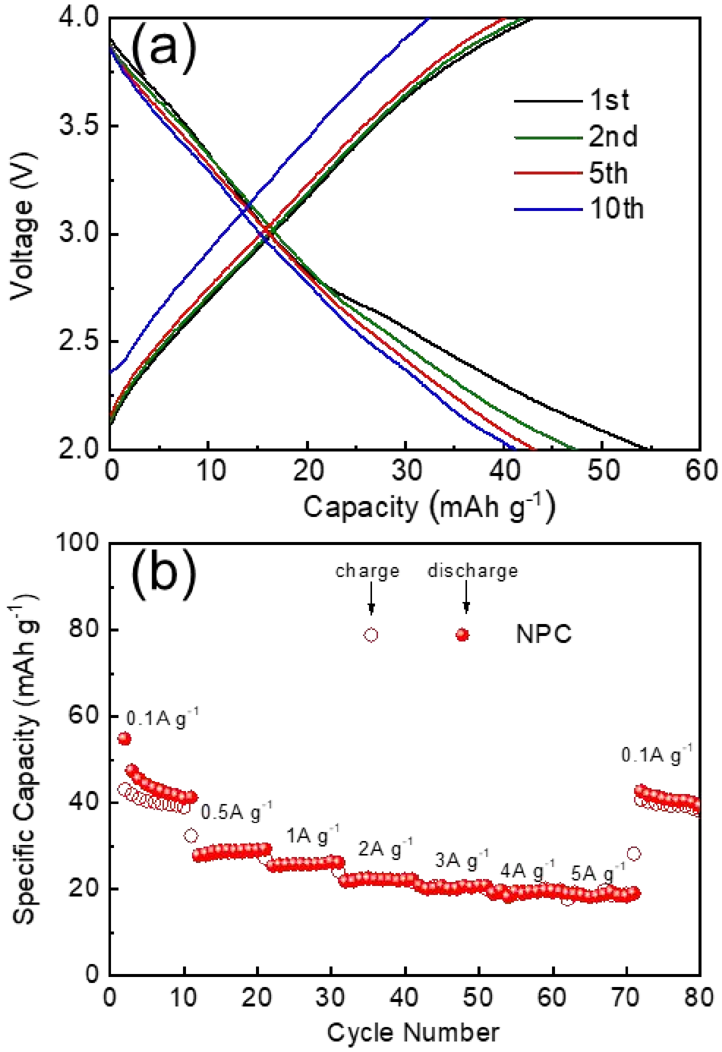

Fig. S16 Electrochemical performance of NPC as PIBs cathode in half cells. (a) Galvonastatic discharge-charge profiles of NPC at 0.1 A g^{-1}; (b) Rate capability of NPC (The preparation process of NPC sample can be found from ref. 1).[1]

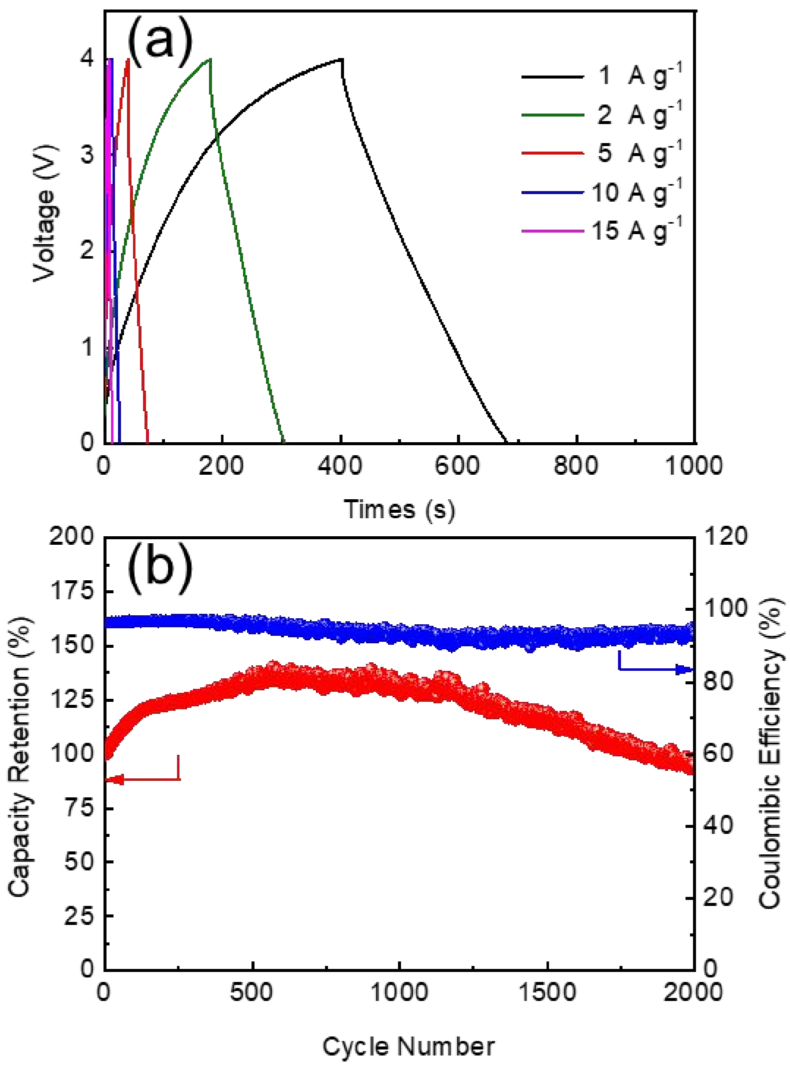

Fig. S17 (a) Representative GCD profiles at different current densities, and (b) cycling stability at 25 A g^{-1} of NBCC//NPC PIHC.

Table S1. Physical parameters of BCC, NBCC, NBCC-L and NBCC-H samples from XRD patterns.

	Highly disordered			Pseudo-graphitic		
	2θ (°)	d_{002}(nm)	Area (%)	2θ (°)	d_{002}(nm)	Area (%)
BCC	21.84	0.406	37.01	23.65	0.376	62.99
NBCC-L	21.74	0.408	54.24	23.60	0.377	46.59
NBCC	21.60	0.410	64.97	23.54	0.378	35.03
NBCC-H	21.55	0.412	69.03	23.42	0.379	30.97

Table S2. Carbon bonding analysis of BCC, NBCC, NBCC-L, NBCC-H.

Binding Energy (eV)	Carbon Bonding	Concentration (%)			
		BCC	NBBC-L	NBBC	NBBC-H
284.4	C=C	76.5	68.15	63.44	57.7
285.9	C-C/C-N	10.69	17.61	24.33	25.93
286.4	C-O	6.75	7.31	7.43	7.34
288.1	C=O	2.28	4.45	2.75	7.04
289.6	COOH	3.79	2.48	2.06	1.99

Table S3. Comparisons of electrochemical performance of NBCC with other carbon anodes for PIBs.

Anode Materials	Rate capability
NBCC (This work)	**499 mAh g^{-1} at 0.05 A g^{-1}** **405 mAh g^{-1} at 0.1 A g^{-1}** **347 mAh g^{-1} at 0.2 A g^{-1}** **278 mAh g^{-1} at 0.5 A g^{-1}** **231 mAh g^{-1} at 1.0 A g^{-1}** **194 mAh g^{-1} at 2.0 A g^{-1}** **134 mAh g^{-1} at 5.0 A g^{-1}** **87 mAh g^{-1} at 10.0 A g^{-1}**
N/S co-doped soft carbon[2]	325mAh g^{-1} at 0.1 A g^{-1} 270 mAh g^{-1} at 0.2 A g^{-1} 241 mAh g^{-1} at 0.5 A g^{-1} 209 mAh g^{-1} at 1.0 A g^{-1} 160 mAh g^{-1} at 2.0 A g^{-1} 115 mAh g^{-1} at 5.0 A g^{-1}
Activated carbon[3]	209 mAh g-1 at 0.1 A g^{-1} 159 mAh g-1 at 0.2A g^{-1} 114 mAh g-1 at 0.4 A g^{-1} 72 mAh g-1 at 0.8 A g^{-1} 30 mAh g-1 at 1.0 A g^{-1}
N-doped hollow carbon[4]	307 mAh g^{-1} at 0.05 A g^{-1} 265 mAh g^{-1} at 0.1 A g^{-1} 246 mAh g^{-1} at 0.2 A g^{-1} 225 mAh g^{-1} at 0.4 A g^{-1} 213mAh g^{-1} at 0.6 A g^{-1} 206 mAh g^{-1} at 0.8 A g^{-1} 200 mAh g^{-1} at 1.0 A g^{-1}

Nano-size porous carbon spheres[5]	208 mAh g^{-1} at 0.05 A g^{-1} 182 mAh g^{-1} at 0.1A g^{-1} 141 mAh g^{-1} at 0.2 A g^{-1} 104 mAh g^{-1} at 0.5 A g^{-1} 81 mAh g^{-1} at 1.0 A g^{-1} 51 mAh g^{-1} at 2.0 A g^{-1}
N/O co-doped carbon hollow multihole bowls[6]	377 mAh g^{-1} at 0.1 A g^{-1}, 305 mAh g^{-1} at 0.2 A g^{-1}, 249 mAh g^{-1} at 0.5 A g^{-1}, 216 mAh g^{-1} at 1.0 A g^{-1}, 182 mAh g^{-1} at 2.0 A g^{-1}
honeycomb-like N-doped carbon[7]	367 mAh g^{-1} at 0.05 A g^{-1}, 324 mAh g^{-1} at.0.1 A g^{-1}, 248 mAh g^{-1} at 0.2 A g^{-1}, 210 mAh g^{-1} at 0.5A g^{-1} 162 mAh g^{-1} at 1.0A g^{-1} 123 mAh g^{-1} at 2.0A g^{-1} 103 mAh g^{-1} at 5.0A g^{-1} 91 mAh g^{-1} at 10.0A g^{-1}
3D porous carbon[8]	175 mAh g^{-1} at 0.05 A g^{-1}, 150 mAh g^{-1} at 0.1 A g^{-1}, 118 mAh g^{-1} at 0.2 A g^{-1}, 93 mAh g^{-1} at 0.4 A g^{-1}, 70 mAh g^{-1} at 0.8 A g^{-1},
N-doped soft carbon [9]	293 mAh g^{-1} at 0.05 A g^{-1}, 266 mAh g^{-1} at 0.1 A g^{-1}, 246 mAh g^{-1} at 0.2 A g^{-1}, 216 mAh g^{-1} at 0.5 A g^{-1}, 194 mAh g^{-1} at 1.0 A g^{-1}.

References

[1] Cui Y, Liu W, Lyu Y, et al. All-carbon lithium capacitor based on salt crystal-templated, N-doped porous carbon electrodes with superior energy storage [J]. Journal of Materials Chemistry A, 2018, 6(37): 18276-18285.

[2] Liu Q, Han F, Zhou J, et al. Boosting the potassium-ion storage performance in soft carbon anodes by the synergistic effect of optimized molten salt medium and N/S dual-doping [J]. ACS Applied Materials & Interfaces, 2020, 12(18): 20838-20848.

[3] Tai Z, Zhang Q, Liu Y, et al. Activated carbon from the graphite with increased rate capability for the potassium ion battery [J]. Carbon, 2017, 123: 54-61.

[4] Hong W, Zhang Y, Yang L, et al. Carbon quantum dot micelles tailored hollow carbon anode for fast potassium and sodium storage [J]. Nano Energy, 2019, 65: 104038.

[5] Zhang H, Luo C, He H, et al. Nano-size porous carbon spheres as a high-capacity anode with high initial coulombic efficiency for potassium-ion batteries [J]. Nanoscale Horizons, 2020, 5(5): 895-903.

[6] Zhang Z, Jia B, Liu L, et al. Hollow multihole carbon bowls: a stress-release structure design for high-stability and high-volumetric-capacity potassium-ion batteries [J]. ACS Nano, 2019, 13(10): 11363-11371.

[7] Li J, Li Y, Ma X, et al. A honeycomb-like nitrogen-doped carbon as high-performance anode for potassium-ion batteries [J]. Chemical Engineering Journal, 2020, 384: 123328.

[8] Li H, Cheng Z, Zhang Q, et al. Bacterial-derived, compressible, and hierarchical porous carbon for high-performance potassium-ion batteries [J]. Nano Letters, 2018, 18(11): 7407-7413.

[9] Liu F, Meng J, Xia F, et al. Origin of the extra capacity in nitrogen-doped porous carbon nanofibers for high-performance potassium ion batteries [J]. Journal of Materials Chemistry A, 2020, 8(35): 18079-18086.